International Journal of Heat and Mass Transfer 256 (2026) 127964

Contents lists available at ScienceDirect

International Journal of Heat and Mass Transfer

journal homepage: www.elsevier.com/locate/hmt

Large Eddy Simulation of environmental impacts on mass transport in laboratory-scale vertical farm

Ali A. Ashnani [a,*], Alpo Laitinen [b], Shervin Karimkashi [a], Ville Vuorinen [a], Titta Kotilainen [c], Juha Näkkilä [d], Pasi Herranen [e], Ossi Kaario [a]

[a] Department of Energy and Mechanical Engineering, Aalto University, Otakaari 4, Espoo, P.O. Box 14100, FI-00076 AALTO, Finland
[b] VTT Technical Research Centre of Finland Ltd, Tekniikantie 21, Espoo, 02150, Finland
[c] Natural Resources Institute Finland (Luke), Latokartanonkaari 9, Helsinki, 00790, Finland
[d] Natural Resources Institute Finland (Luke), Itsenäisyyden aukio 2, Turku, 20800, Finland
[e] Department of Bioproducts and Biosystems, Aalto University, Otakaari 4, Espoo, P.O. Box 63000, FI-00076 Aalto, Finland

ARTICLE INFO

Keywords:
Vertical farm
Indoor plant factory
CEA
Ventilation
Environmental effect
CFD
LES

ABSTRACT

The impact of environmental factors on airflow and mass transport within a laboratory-scale vertical farm is investigated using Computational Fluid Dynamics. Large Eddy Simulation models complex airflow behaviour, while solving enthalpy and mass transport equations yields temperature, humidity, and CO_2 concentration. The Eulerian-Lagrangian approach simulates the free-fall of water droplets in the dehumidifier-cooling system. Humidity and CO_2 consumption/production by plants and utilities are modelled as volumetric sources/sinks. An experimental campaign is conducted to measure temperature, relative humidity, and CO_2 above cultivation beds, validating the numerical setup with mean absolute errors of 0.8%, 2.2%, and 3.9%, respectively. Analysing the airflow shows that the free fall of droplets is the dominant mechanism driving airflow characteristics. We investigate the effects of wall confinement, number of lamps, and location of lamps on the mass transport. Curtains were used to divide each cultivation bed into three regions to assess the wall confinement effect. Results show the overall adverse effect of curtains on mass transport. In more detail, mass transport is enhanced when the curtains and streamlines are aligned parallel, whereas it is reduced when they are perpendicular. Increasing the number of operative lamps improves the uniformity of mass distribution on the upper cultivation beds due to a stronger positive buoyancy. Positioning lamp-induced buoyant flow within the droplet's lateral momentum injection zone further enhances vertical mass transport. These findings highlight the impact of environmental factors on mass transport, offering insights for more efficient designs of indoor vertical farms.

1. Introduction

Rising concerns about food security, water scarcity, and climate change drive us towards more advanced farming methods. Indoor Vertical Farm with Artificial Lighting (IVFAL) offers the potential to produce more agricultural products with lower CO_2 emissions, land and water usage compared to traditional agricultural methods [1–3]. IVFAL systems employ a controlled environment agriculture (CEA) method. This method adjusts the plant-affecting factors to an optimal range for plant growth. The primary plant-affecting factors are light, CO_2, RH, temperature, and air velocity [1,4,5]. Correspondingly, utilities such as artificial lighting sources, CO_2 supplier, dehumidifier, and fans need to be positioned within the vertical farm to control such plant-affecting factors. However, controlling these plant-affecting factors via the mentioned utilities leads to a higher energy demand of IVFAL compared to traditional agriculture [2]. In particular, while wind and sunlight are freely available in conventional farming, IVFAL systems rely on energy-intensive utilities, such as mechanical ventilation and artificial lighting, to maintain the optimal plant growth condition. This reliance on energy-demanding utilities leads to a challenge on energy consumption in IVFALs.

Based on the type of agricultural system, there are different solutions to address the uniformity of plant-affecting factors. In a greenhouse, utilising new cooling technologies, sun shading curtains, and mechanical ventilation optimise the uniformity of temperature and humidity [6,7]. In IVFALs, however, as the system is closed, sunlight does not affect the internal temperature. Moreover, the isolated walls hinder internal/external mass and heat exchange. Consequently, the system requires CO_2 supplier, a dehumidifier, artificial lighting for

* Corresponding author.
E-mail address: ali.ashnani@aalto.fi (A.A. Ashnani).

https://doi.org/10.1016/j.ijheatmasstransfer.2025.127964
Received 8 July 2025; Received in revised form 22 September 2025; Accepted 12 October 2025
Available online 23 October 2025

photosynthesis, a cooling system to mitigate the heat waste of artificial lighting, and adequate airflow velocity above cultivation beds for mass exchange of canopies. The level of CO_2, RH, and temperature above the cultivation beds depends strongly on the airflow [8]. Airflow is one of the most critical factors for optimising the vertical farming systems. In this regard, Thongbai et al. [4] experimentally investigated the effect of CO_2 and air circulation on the photosynthetic and transpiration rate of tomato seedlings. They concluded that the impact of increasing either the CO_2 concentration from 273 to 545 µmol/mol or velocity from 0.3 to 1 m/s results in a similar enhancement of the net photosynthetic rate by 67%–76%. Moreover, Ahmed et al. [9] provided a literature survey on suitable environmental conditions for lettuce growth in CEA systems with artificial lighting. Based on their review study, the optimum range of velocity, RH, CO_2, and temperature correspondingly are 0.3–0.7 m/s, 70%–80%, 1000-1500 µmol/mol, and 18–25 °C. Although the optimum ranges of plant-affecting factors have been extensively studied in the literature, achieving such optimum ranges in IVFAL systems still requires further studies.

The first step to optimise the ventilation of IVFALs is to acquire the mentioned plant-affecting factors; temperature, carbon dioxide, relative humidity and airflow inside the system. Computational Fluid Dynamics (CFD), as a strong numerical tool for solving the fluid flow governing equations, offers comprehensive results regarding aforementioned factors. CFD offers significant advantages in cost-per-data efficiency, compared to traditional experiments. Particularly, CFD manifests its capability to simulate various agricultural buildings, including vertical farming systems [10]. Therefore, CFD studies have focused on optimising the ventilation of vertical farming systems to find the suitable range of the factors along with a homogeneous distribution above cultivation beds [11–13]. In what follows, CFD studies are briefly reviewed, which have mainly focused on mechanical ventilation configuration effects on the airflow in vertical farming systems.

Several CFD studies have utilised Reynolds Average Navier Stokes (RANS) turbulence modelling approach to simulate the ventilation inside the IVFAL. Lim and Kim [14] analysed numerically the airflow pattern in a vertical farm by changing the locations of the velocity inlet and outlet, utilising the Realisable k-ε turbulence model. They concluded that the location of the velocity inlet and outlet has a great influence on the airflow pattern. Additionally, Zhang et al. [15] conducted a CFD study on airflow uniformity in a single shelf food production system by investigating various air jet nozzle configurations employing the standard k-ε model. They concluded that the multi-jet perforated air tube is more suitable for providing airflow than horizontal fans, especially for the centre of cultivation beds. In this regard, Fang et al. [16], in their CFD study, evaluated the airflow uniformity by proposing three design configurations of over-headed perforated air tubes, varying nozzle diameters and distances between nozzle holes on the air tube. More recently, Zhang and Kacira [17] considered various scenarios with different air-tube configurations and analysed the airflow uniformity in an IVFAL by implementing porous media to simulate lettuce canopies, considering the transpiration and using the standard k-ε turbulence model. In another study, Naranjani et al. [18] explored the velocity uniformity based on changing the location of the airflow inlet/outlet in an IVFAL, by considering photosynthesis-induced mass transport and the RNG k-ε turbulence model. In addition, Sohn et al. [19] simulated four cases with different airflow inlet/outlet sizes in a vertical farm by utilising the standard k-ε. They concluded that the location of the airflow inlet/outlet can significantly change the airflow pattern within the system. Also, Larochelle Martin and Monfet [20] proposed two optimised designs for the airflow inlet by simulating a vertical farm system with the k-ε turbulence model. Most of the aforementioned studies had considered the heat release of artificial lighting systems [12,15–18], without simulating the dehumidifier and cooling system. Agati et al. [21], however, incorporated dehumidifiers and evaporators into their simulation of vertical farming ventilation to analyse the thermo-fluid dynamic behaviour in greater detail. They used the Realisable k-ε turbulence model in their simulation. Additionally, they evaluated the Absolute Error (AE) for RH and temperature on two floors of the vertical farm based on their experimental measurements. The reported averaged AEs were 5.3% and 5.0% for RH, and 3.1% and 3.9% for temperature, for the two different floors, respectively.

As discussed above, and based on the literature survey of Larochelle Martin and Monfet [20], and Bournet and Boulard [22], most of the CFD simulations of greenhouses and vertical farms are conducted with the RANS turbulence modelling approach. LES turbulence approach, however, manifests its capability to provide more accurate and reliable results compared to RANS [23]. Whereas, RANS models are unable to provide detailed information on instantaneous turbulent flows [24]. Korhonen et al. [25] simulated the indoor ventilation using LES turbulence model. Their results highlight the significant effect of airflow-obstacle interaction on the ventilation and the effect of airflow on CO_2 propagation. Despite the demonstrated advantages of the LES approach in modelling indoor ventilation, it has not been utilised in the literature of the indoor vertical farm systems.

Considering the aforementioned literature survey, the aim of the present study is to fill two identified major gaps in the CFD studies on indoor vertical farm ventilation. First, most previous studies have used RANS turbulence models, or simplified the flow as laminar. To the best of our knowledge, LES has not been previously used in IVFAL simulations. Second, the majority of prior CFD studies have focused on the ventilation configuration effect in a momentum-driven medium, while the effect of wall confinement and buoyancy-driven flows in a density-driven medium remains largely unexplored. To address these research gaps, the present study aims to achieve the following objectives:

(1) Conduct an experimental campaign, measuring temperature, CO_2, and relative humidity in a vertical farm.
(2) building a LES simulation setup based on a real laboratory-scale vertical farm physics and geometry to:
    - Assess the accuracy of the simulation results for temperature, CO_2, and relative humidity,
    - Analyse the behaviour of the instantaneous airflow, and its interaction with mass transport.
(3) Implement curtains normal to the cultivation beds to assess the effect of wall confinement on airflow within the computational domain.
(4) Adjust the number of active LEDs (heat sources) and shift their location to investigate the interaction of buoyancy and airflow within the system.
(5) Model the cooling and drying processes in a dehumidifier by source terms and free-falling droplets.

2. Methodology

This study was conducted based on the laboratory-scale vertical farm of the Natural Resources Institute Finland (LUKE) located in Piikkiö research infrastructure, Finland. Along with CFD simulations, we carried out an experimental campaign in the vertical farm to validate our numerical setup. The methodology details both the numerical configuration and the experimental measurements process.

2.1. Numerical procedure

Here, we first describe the geometry of the simulated vertical farm, along with the utilities and their roles within the system. Second, we provide governing equations for the CFD simulation, and ultimately, present the Boundary Condition (BC) and numerical simplifications.

2.1.1. Geometry and utilities

Fig. 1(a) presents a 3D view of the computational domain, illustrating the volumetric sources and sinks, the locations of LED lamps, curtains and the dehumidifier. Coloured boxes in the figure highlight the locations of volumetric sources and sinks, which are discussed further in Section 2.1.3. The vertical farm occupies a total volume of 131.8 m^3 with dimensions 2.6 m, 7.8 m and 6.5 m, in height, length and width, respectively. It includes two shelf structures, each supporting two trays on different floors, designated for the cultivation beds. Plants on these cultivation beds release humidity and absorb CO_2 through transpiration and photosynthesis. A CO_2 supplier pipe is positioned in the middle of two shelves at the base floor, and the dehumidifier is located alongside the shelves. Thirty-six LED lamps supply the light required for photosynthesis of the plants. Seven nozzles in the dehumidifier region release water droplets into the system with zero initial velocity, free-fall. The heat exchange of these droplets with air reduces the air temperature below its dew point, causing water vapour to condense onto the droplets and leading to dehumidification of the air. Additionally, two curtains separate cultivation beds and manipulate the airflow within the system. In what follows, the governing equations and numerical configurations for simulating the mentioned utilities are presented. Fig. 1(b) illustrates horizontal and vertical slices in the computational domain. xy1 and xy2 are located 15 cm above the cultivation beds on the first and the second floors, respectively. zy1 and zy2 planes represent vertical cross-sections along the shelves, far from and close to the dehumidifier, respectively. zy3 plane represents a vertical cross-section along the dehumidifier system. Moreover, the vertical planes zx1, zx2 and zx3 provide lateral planes of the cultivation beds, providing a complementary explanation in the supplementary material.

2.1.2. Governing equations

The main governing equations include the continuity equation, Navier-Stokes Equations (NSE), and the heat and mass transport equations. We applied a Smagorinsky-type LES [26] on the governing equations to model the turbulence behaviour of the flow. Consequently, the equations are represented with spatial filtering (Δ). Eqs. (1) and, (2) represent the continuity and NSE equations as:

$$\frac{\partial \rho}{\partial t} + \frac{\partial \rho \tilde{u_i}}{\partial x_i} = 0, \tag{1}$$

$$\frac{\partial \rho \tilde{u_i}}{\partial t} + \frac{\partial \rho \tilde{u_i} \tilde{u_j}}{\partial x_i} = -\frac{\partial p}{\partial x_i} + \frac{\partial}{\partial x_j}\left[\rho \nu \left(\frac{\partial \tilde{u_j}}{\partial x_j}\right)\right] + \frac{\partial \tau_{ij}^{sgs}}{\partial x_j} + (\rho g - F_D)\delta_{i3}, \tag{2}$$

Here, ρ, ũ, g, F_D and ν are density, spatially filtered velocity, gravitational acceleration, drag force, and molecular kinematic viscosity, respectively. The indices i and j follow Einstein notation, corresponding to the x, y, and z spatial directions. Additionally, δ denotes the Kronecker delta, and its index, i3 implies the existence of the gravity and drag force term exclusively in the z direction. The third term, τ^{sgs} is the Sub-Grid-Scale (SGS) stress tensor, which accounts for large eddies diffusion and requires modelling. The SGS stress tensor, τ^{sgs}, is modelled as shown in Eq. (3);

$$\tau_{ij}^{sgs} = \frac{2}{3} k_{sgs} \delta_{ij} - C_k k_{sgs}^{(1/2)} \Delta \left(\frac{\partial \tilde{u_j}}{\partial x_i} + \frac{\partial \tilde{u_i}}{\partial x_j}\right), \tag{3}$$

where Δ is the spatial filter width defined as the cube root of the cell volume, C_k is the model constant set to 0.094, and k_{sgs} represents the subgrid-scale turbulent energy and obtained from the k-equation presented in Eq. (4);

$$\frac{\partial \rho k_{sgs}}{\partial t} + \frac{\partial \rho k_{sgs}}{\partial x_j} - \frac{\partial}{\partial x_j}\left[\rho\left(\nu + \nu_{sgs}\right)\frac{\partial k_{sgs}}{\partial x_j}\right] = -\frac{1}{2}\rho \tau_{ij}^{sgs}\left(\frac{\partial \tilde{u_j}}{\partial x_i} + \frac{\partial \tilde{u_i}}{\partial x_j}\right) - C_\epsilon \frac{\rho k_{sgs}^{3/2}}{\Delta}, \tag{4}$$

Considering the default value of the dissipation constant C_ϵ as 1.048, and calculating sub-grid scale viscosity ν_{sgs} as;

$$\nu_{sgs} = C_k \Delta \sqrt{k_{sgs}}, \tag{5}$$

The only remaining term from NSE is the drag force resulting from air resistance confronting the droplets' free-fall. Assuming that droplets preserve a spherical shape throughout their descent, the drag force can be calculated as;

$$F_D = \frac{3}{4}\frac{\nu \rho C_D Re_d}{\rho_d d^2} \tag{6}$$

where C_D, Re_d, ρ_d, and d correspond to the drag constant, droplet Reynolds number, droplet density, and the diameter of the droplets which is equal to 3 mm, respectively. The drag constant is calculated as Eq. (7):

$$C_D = \frac{24}{Re_d}\left(1 + \frac{1}{6} Re_d^{2/3}\right) \quad , \tag{7}$$

if $Re_d > 1000$, otherwise it is set to a constant value of 0.424. Re_d defines as Eq. (8);

$$Re_d = \frac{|u_{rel}|\, d}{\nu} \tag{8}$$

Which depends on droplet diameter, the magnitude of relative velocity between the droplet and the airflow $|u_{rel}|$, and the kinematic viscosity of air. Calculating Eqs. (6) to (8), the drag force term of NSE gains closure. However, the density varies with the temperature, and consequently, the temperature field needs to be solved. For acquiring the temperature field, the enthalpy advection–diffusion equation was solved as Eq. (9);

$$\frac{\partial \rho h}{\partial t} + \frac{\partial \rho h \tilde{u_j}}{\partial x_i} + \frac{\partial \rho K}{\partial t} + \frac{\partial \rho K \tilde{u_j}}{\partial x_i} - \frac{\partial p}{\partial t} = -\frac{\partial q}{\partial x_j} + \frac{\partial \tau_{ij} u_j}{\partial x_j} + \rho r + \rho g \delta_{i3} u_3, \tag{9}$$

where h and K are enthalpy and specific kinetic energy. q, and τ are heat flux, and the viscous term of the NSE, r is the mass-specific heat source, and the last term represents the gravitational work. Adding the ideal gas assumption for airflow gives the full closure that provides the Temperature field from the enthalpy. Moreover, the NSE are coupled with the enthalpy equation by density correction based on the ideal gas law;

$$\rho = \frac{p}{RT}, \quad dh = c_p dT, \tag{10}$$

where T is the temperature, p is the thermodynamic pressure, and c_p and R are specific gases and the specific heat capacity at constant pressure, respectively.

Acquiring CO_2, and H_2O requires solving advection–diffusion equations for concentration;

$$\frac{\partial \rho c}{\partial t} + \frac{\partial \rho \tilde{u_j} c}{\partial x_i} = \frac{\partial}{\partial x_j}\left[\Gamma\left(\frac{\partial \rho c}{\partial x_j}\right)\right] + S_c, \tag{11}$$

where c denotes to the concentration of CO_2, or H_2O, S_c is the sink/source term, and Γ is mass diffusion can be calculated with Schmidt number, $Sc = \nu/\Gamma$. Solving Eqs. (1) to (6) provides the required fields for evaluating the fluid flow characteristics within the vertical farm system.

The mathematical procedure and numerical schemes in the current study resemble the CFD ventilation study of Laitinen et al. [27]. We utilised `rhoPimpleFoam` solver in the OpenFoam V10 software. The solver was described as a transient solver for simulating compressible turbulence flows in HVAC applications.

2.1.3. Boundary conditions and simplifications

Next, we discuss the details of boundary conditions, volumetric source/sink implementation, and their corresponding simplifications. The volumetric sinks and sources within the system have been shown in Fig. 1(a). Thirty-six lamps provide the artificial light for photosynthesis in the physical system. A constant heat flux of 20 W has been set on

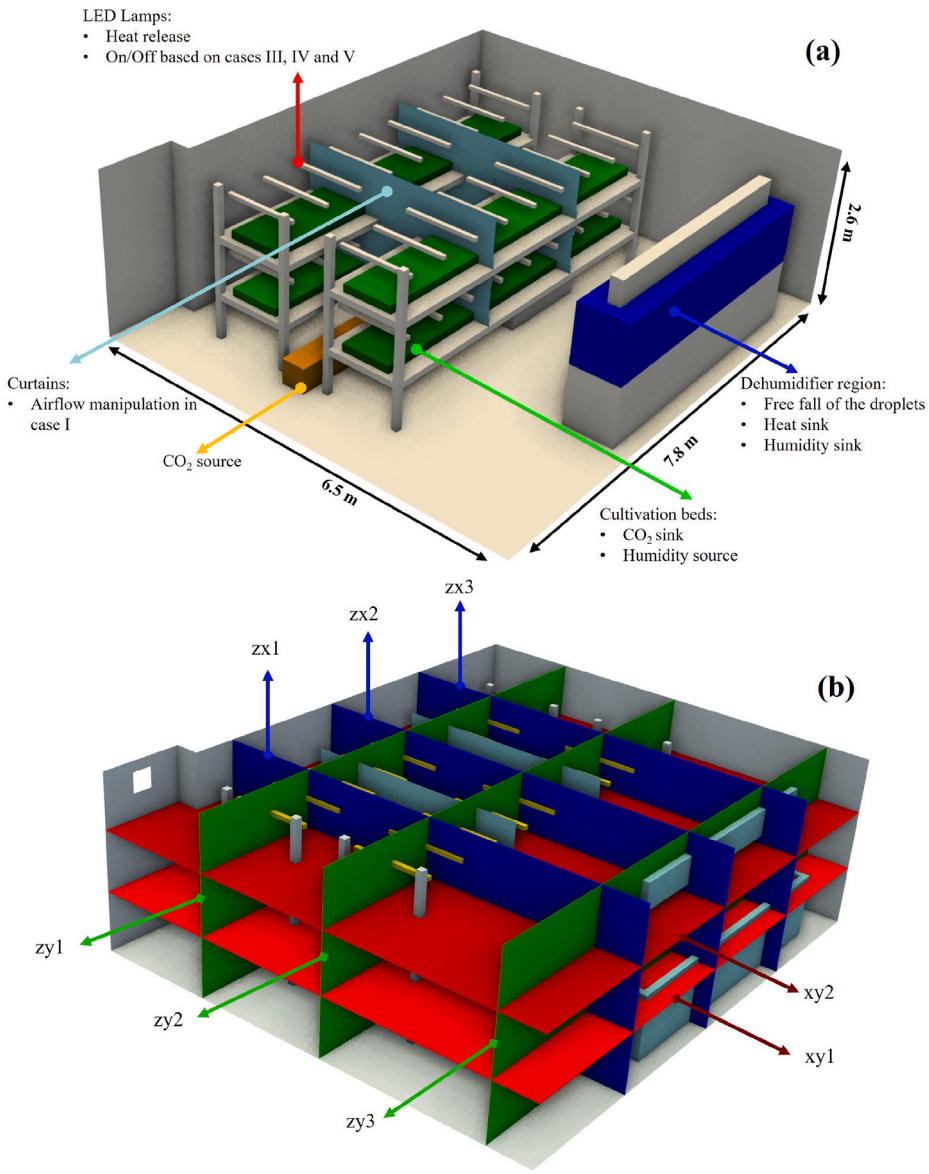

Fig. 1. 3D view of the computational domain, showing volumetric sinks/sources, curtains for air flow manipulation, and lamps for photosynthesis. (b) Illustration of the 2D cross-section planes. (For interpretation of the references to colour in this figure legend, the reader is referred to the web version of this article.)

the boundaries of the lamps in the computational domain to simulate their heat release. To reduce computational complexity, the effect of radiation was neglected. By considering the order of magnitude of the ratio of radiation heat transfer (Q_r) to convection heat transfer (Q_{conv}):

$$\frac{Q_r}{Q_{\text{conv}}} = \frac{\varepsilon\sigma\left(T^4_{\text{surface}} - T^4_{\text{ambient}}\right)}{h\left(T_{\text{surface}} - T_{\text{ambient}}\right)}, \tag{12}$$

where ε and σ are emissivity and Boltzmann coefficient with the order of magnitude of $O(\varepsilon) = 1$ and $O(\sigma) = 10^{-8}$, considering the order of magnitudes of temperature difference between the surface and ambient as $O(T_{\text{surface}} - T_{\text{ambient}}) = 10$ and $O(T^4_{\text{surface}} - T^4_{\text{ambient}}) = 10^9$ alongside the natural convective heat transfer $O(h) = 10$, the order of magnitude of convective heat would be ten times greater than the radiation heat transfer. As the results demonstrated a good agreement with the experimental data, justifying this simplification in the context of the present study. The dehumidifier region contains a volumetric sink equivalent to the total heat release of all LED lamps (i.e, 720 W). The photosynthesis and transpiration of plants are simulated by implementing a volumetric source of humidity and volumetric sink of CO_2 in rectangular boxes on the cultivation beds where the height of volumetric sinks and sources are 15 cm, depicted in green colour in Fig. 1(a).

In the physical vertical farm, the CO_2 distributor pipe was in the middle of two shelves on the floor, supplying CO_2 for plant photosynthesis. CO_2 distributor pipe is simplified and simulated as a volumetric source of CO_2 in the same location. The CO_2 release by the volumetric source is equivalent to the consumption rate of CO_2 on cultivation beds. The rate of transpiration is simplified to be constant, similar to the greenhouse CFD study of Piscia et al. [28], and the humidity production above the cultivation bed is equivalent to the humidity consumption in the dehumidifier region. Both CO_2 and humidity are considered as passive scalars with arbitrary values.

The inlet fan (very low mass flow) has a uniform velocity of 0.01 m/s, and the outlet BC alternates between zero gradient velocity when the flow aims to exit the system, and zero velocity. When the flow aims to exit the system, the BC acts as an outlet, while in a backwards-flow, it acts as a wall with no-slip BC, similar to a check valve. The outlet has been implemented in the computational domain to maintain the pressure balance. All the walls and structures, including

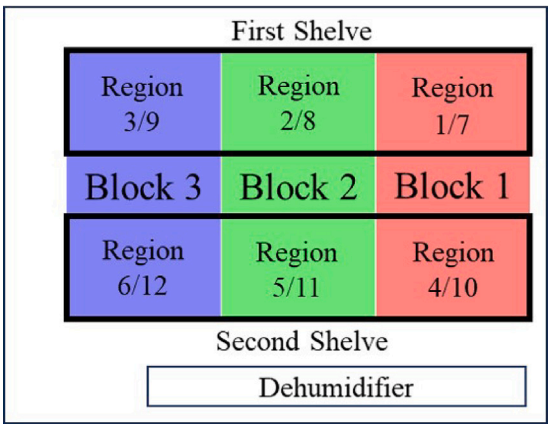

Fig. 2. The schematic of the upper view of the system with the specification of elements in the system with geometrical classifications based on Blocks and Regions (R). Each block contains four regions, two on the first floor and two on the second floor. In each block, the first mentioned region in texts from left to right belongs to regions of the first and second floor (e.g., Region 1/7 means Region 1 on the first floor and Region 7 on the second floor).

Table 1
Matrix of simulations.

Case	Blocks with active LEDs	Curtains
Case I	All	With
Case II	All	Without
Case III	1–2	Without
Case IV	1–3	Without
Case V	2–3	Without

the dehumidifier pool, water tanks, and shelf, have no-slip boundary conditions.

In the physical dehumidifier, droplets are released into the system at a lower temperature than the air to balance the heat release of lamps and free-fall into the dehumidifier pool. This heat exchange results in a lower air temperature than the dew point, causing condensation and consequently, air dehumidification. In the simulation, the nozzle of the dehumidifier releases droplets with zero velocity, and they fall due to the gravitational force into the dehumidifier pool. Heat and humidity volume sinks are implemented in the dehumidifier region to model the droplets-air heat exchange and dehumidification process. The curtains were originally installed in the LUKE laboratory-scale vertical farm as shadow curtains to block light among the samples on the cultivation beds. As we conduct our experimental campaign in the same vertical farm, our validation case (case I) includes the implementation of curtains with no-slip boundary conditions.

There are in total four cultivation beds in the vertical farm. To facilitate addressing zones in these cultivation beds, we introduced location indicators; blocks and regions in the top-view schematics of the system, Fig. 2. Location references are labelled as Block 1 to 3, and Regions 1 to 12 in Fig. 2. Two curtains divide the cultivation beds into three zones, which through the present study will be referred to as blocks. As each block covers a segment of the four cultivation beds, categorising each block by the cultivation beds provides the reference labels for Regions. In Fig. 2, the first and second numberings in the format of Region x/y receptively indicate regions on the first and second floor. Therefore, regions 1 to 6 are located on the first floor, while 7 to 12 are positioned on the second floor.

Table 1 provides the characteristics of simulated cases. Case I, the validation case, has a setup similar to that of the experimental campaign. In this case, curtains are implemented, and all LED lamps are active (cf. Fig. 1). Case II is similar to Case I, but without curtains to evaluate the effect of curtains. Cases III to V, termed light arrangement cases, with operative LED lamps in only two of three blocks (cf. Fig. 2). In Case III, LED lamps are active in blocks 1 and 2; in Case IV, in blocks 1 and 3; and in Case V, in blocks 2 and 3. These light arrangement cases are designed to evaluate the effect of lamp location in the vertical farm

2.1.4. Grid resolution assessment

Three grid resolutions have been simulated to evaluate the grid sensitivity. The 5% deviation of CO_2, temperature and velocity has been opted for grid sensitivity evaluation. This criterion was met by all the aforementioned factors in the medium grid. The deviations between medium grid and fine grid, with 14.1×10^6 and 32.2×10^6 cells, for velocity, temperature and CO_2 found to be 0.66%, 2.02%, and 3.23%, subsequently. Consequently, the medium grid has been utilised for the simulation. The grid study is discussed in detail in the supplementary material. Additionally, the ratio of the resolved Turbulent Kinetic Energy (TKE) to the total TKE is investigated to ensure the sufficiency of the LES mesh resolution. Moreover, for wall treatment, a y^+ insensitive wall function has been used for wall modelling. The grid resolution and refinement regions are further discussed in the supplementary material.

2.2. Experimental measurements

In addition to the numerical simulations, we conducted an experimental campaign at the Piikkiö research infrastructure by LUKE IVFAL. This campaign was designed to obtain the measurements for validating the CFD setup. The campaign was carried out after the simulations to serve as a blind validation, thereby enhancing the reliability of the numerical data. Data were collected using six Wave Plus probes of Airthings ASA. Each probe collects data for CO_2 with a Non-Dispersive Infrared gas detector system and reports RH level and temperature every 5 min with the accuracies of ±3%, and ±0.5 °C, respectively. The probes were positioned on the shelves of the first floor, with each bed divided into three blocks and a probe placed at the centre of each block. Data collection spanned three days, with the periods lasting 1, 2, 3, and 9 h. During these measurements, all LED lamps remained operational, CO_2 injection was maintained with two-hour pause intervals, and the cooling system operated continuously. Ultimately, the experimental data were used for CFD simulation validation by comparing temperature, CO_2 concentration, and RH level measurements with the simulated values at matching locations (Table 2).

3. Results and discussion

3.1. Validation

As detailed in Section 2.2, six probes were positioned at the middle of each block during the experimental campaign to measure absolute error of RH, CO_2, and temperature. In the simulation case I, these properties were time-averaged at the middle of each cultivation bed on the first floor and compared to the experimental data, as presented in Table 2. The MAE for RH, CO_2, and temperature are 2.00%, 3.92%, and 0.82%, respectively. This result demonstrates the good agreement between the simulation data and the experimental data.

3.2. General observation

This subsection presents CO_2 propagation among all cases I to V visualised through 3D volume rendering in Fig. 3(a) to (e). The legend bar depicts the highest and the lowest CO_2 concentrations are illustrated, while the medium levels of 1075 ppm to 1175 ppm are not illustrated in the figure. The CO_2 concentration is lower on the second floor for all cases. In case I, lower accumulation of CO_2 can also be observed on the first floor. The highest CO_2 levels can be seen on the base floor where the CO_2 supplier is located. It can be observed that this high concentration of CO_2 inclines towards the dehumidifier region. In general, curtains show an adverse impact on the mass transport within the system as the micro-climates (zones with the lowest CO_2 concentration) are detectable in both floors.

Table 2
Validation of LES simulation based on case I compared to experimental data. Absolute Errors (AE) are provided for each region on the first floor of cultivation beds, and MAE is presented for RH, CO_2, and temperature.

Region	RH [–]			CO_2 [ppm]			Temperature [K]		
	Exp.	LES	AE (%)	Exp.	LES	AE (%)	Exp.	LES	AE (%)
1	73.26	69.87	4.85	1090.3	1053.25	−3.52	292.92	289.89	−1.04
2	72.38	73.39	1.38	1089.96	1054.54	−3.36	291.90	289.74	−0.74
3	73.73	72.93	−1.09	1076.09	1033.80	−4.09	292.51	289.65	−0.99
4	67.96	68.19	0.34	1114.68	1099.53	−1.38	292.63	289.95	−0.93
5	65.42	67.56	3.17	1085.79	1187.69	8.58	291.17	289.80	−0.47
6	67.29	68.09	1.18	1054.81	1082.82	2.59	291.90	289.69	−0.76
MAE		2.00			3.92			0.82	

3.3. Airflow in case I

In this subsection, we describe general airflow characteristics and their effect on mass transport by investigating instantaneous velocity fields in Case I. To illustrate the instantaneous velocity, we define 2D cross-sectional planes and label them in Fig. 2(b) for future reference.

Fig. 4(a–c) depict the instantaneous airflow velocity on the vertical cross-sections zy3, zy2, and zy1, respectively. It is observed that the velocity magnitude in the dehumidifier region (zy3) (maximum velocity 3.23 m/s) is larger than that of the other regions. Therefore, for better visualisation, a different colour scale is used in Fig. 4(a). Moreover, the water tanks are indicated on the base floor in Fig. 4(b) and (c). In the actual vertical farm, these water tanks serve as suppliers of nutrients for the plants via the hydroponic method. In the current study, however, they are merely considered as structures with the wall boundary condition. In addition, Roman numerals identify different zones of interest in the figures to facilitate the corresponding description of the zones.

By classifying the momentum transport into vertical and horizontal circulations, it will be possible to provide a better description of the airflow transport within the system. Here, we start by describing vertical circulation, then horizontal circulation, and finally, their effects on mass transport.

3.3.1. Vertical airflow mechanisms

Two major mechanisms assist in the vertical flow of air from the second to the first floor in the dehumidifier zone, cf. Fig. 4(a). These two mechanisms are the air-droplet shear stress exchange and the negative buoyancy in the dehumidifier/cooling zone. To describe the momentum exchange mechanisms in the dehumidifier region, we employed the terminology used for jet flows. In this context, the axial momentum exchange refers to the exchange of momentum parallel to the jet flow stream, while the lateral momentum exchange indicates the exchange of momentum perpendicular to the jet flow stream.

The first observed mechanism in Fig. 4, i.e. the air-droplet shear stress exchange, contains three distinguishable momentum transport events in the dehumidifier region: (i) the primary momentum transport from the water droplets to air, (ii) the lateral secondary airflow momentum exchange of high-velocity and low-velocity airflows, and (iii) the axial secondary airflow at the bottom of the dehumidifier pool towards the upper levels. The shear stress between the high-velocity water droplets and the low-velocity adjacent air leads to the momentum transfer from the water droplets to the airflow (i). Consequently, airflow tends to follow the droplets' path beneath the nozzles towards the dehumidifier pool, forming seven columns of jet-like primary airflow, cf. Fig. 4(a). This primary flow results in two secondary flows, which are here referred to as the lateral and axial secondary flows.

The axial secondary flow emanates from the floor of the dehumidifier pool confinement. When the primary flow hits the dehumidifier's impermeable floor. Airflow tends to horizontally redirect its path rather than flowing upward and overcome the downward momentum force. Consequently, it can be seen in the first jet, from left to right, that velocity travels towards the wall of the dehumidifier pool and then redirects upward (iii), while for the other jets, there is no space for horizontal redirecting and the airflow inevitably confronts the downward primary airflow. The boundaries of the jets undergo shear instabilities due to the sharp velocity gradient on the jet boundaries which this confrontation of the primary airflow and the axial secondary airflow further destabilises the boundaries of the jet.

This shear stress instability causes the emergence of the lateral secondary flow (iii). The lateral secondary flow is called the entrainment/injection mechanism, leading to the horizontal circulation in the system. The schematic of this mechanism is shown in Fig. 4(S) and further explained in Fig. 6.

The second mechanism responsible for the vertical circulation is buoyancy, cf. Fig. 4(b) inset iv. While the dehumidifier/cooling system results in negative buoyancy, the LEDs cause positive buoyancy. The effect of LEDs on the airflow is indicated in the longitudinal cross-sections of the cultivation beds, i.e. the zy2 and zy1 planes in Fig. 4(b) and (c). The positive buoyant flow on the first floor gets trapped by the second-floor cultivation bed, travels towards the edges of the bottom part of the second-floor cultivation beds and then travels upward (v), resulting in temperature stratification within the system (Fig. 5). As there are two groups of LEDs for each floor, two different height levels of temperature stratification with average temperatures of 293.5 K and 296 K are observed in Fig. 5. The vertical temperature difference within the system is 8 K, while the horizontal temperature distributions over the cultivation beds are rather homogeneous (not shown for brevity). As a consequence of negative and positive buoyancy, the temperature near the ceiling does not exceed 300 K while the temperature of the floor is maintained above 290 K, cf. Fig. 5.

To conclude, the LED-induced positive buoyancy, along with the dehumidifier-induced negative buoyancy and shear stress transport, generate a vertical circulation within the system. Furthermore, the interaction of these mechanisms leads to higher velocity magnitudes on the cultivation beds close to the dehumidifier (Fig. 4(b)) compared to the cultivation beds far from it (Fig. 4(c)).

3.3.2. Horizontal airflow mechanisms

Fig. 6(a) and (b) show the instantaneous velocity, 15 cm above the first and second floor cultivation beds, respectively. The aforementioned momentum entrainment/ejection phenomenon (Section 3.3.1) from the dehumidifier results in two noticeable airflows in Fig. 6(a). There is an anticlockwise circulation near the walls of the system on the first floor, which begins from the right side of the dehumidifier (i), circulates around the system close to the outer walls (ii) and rejoins the dehumidifier region from the left side (iii). The high velocity airflow in the vicinity of the middle of the dehumidifier (iv) emerges due to the interaction of the LED-induced positive buoyancy airflow with the negative buoyant flow.

In the second floor, Fig. 6(b), contrary to the first floor, the dehumidifier region is not confined by the dehumidifier pool walls. Consequently, the momentum exchange extends beyond the dehumidifier region. However, the momentum entrainment/injection is higher than that on the second floor due to the greater shear instability of the jet boundaries closer to the dehumidifier wall on the first floor. As a

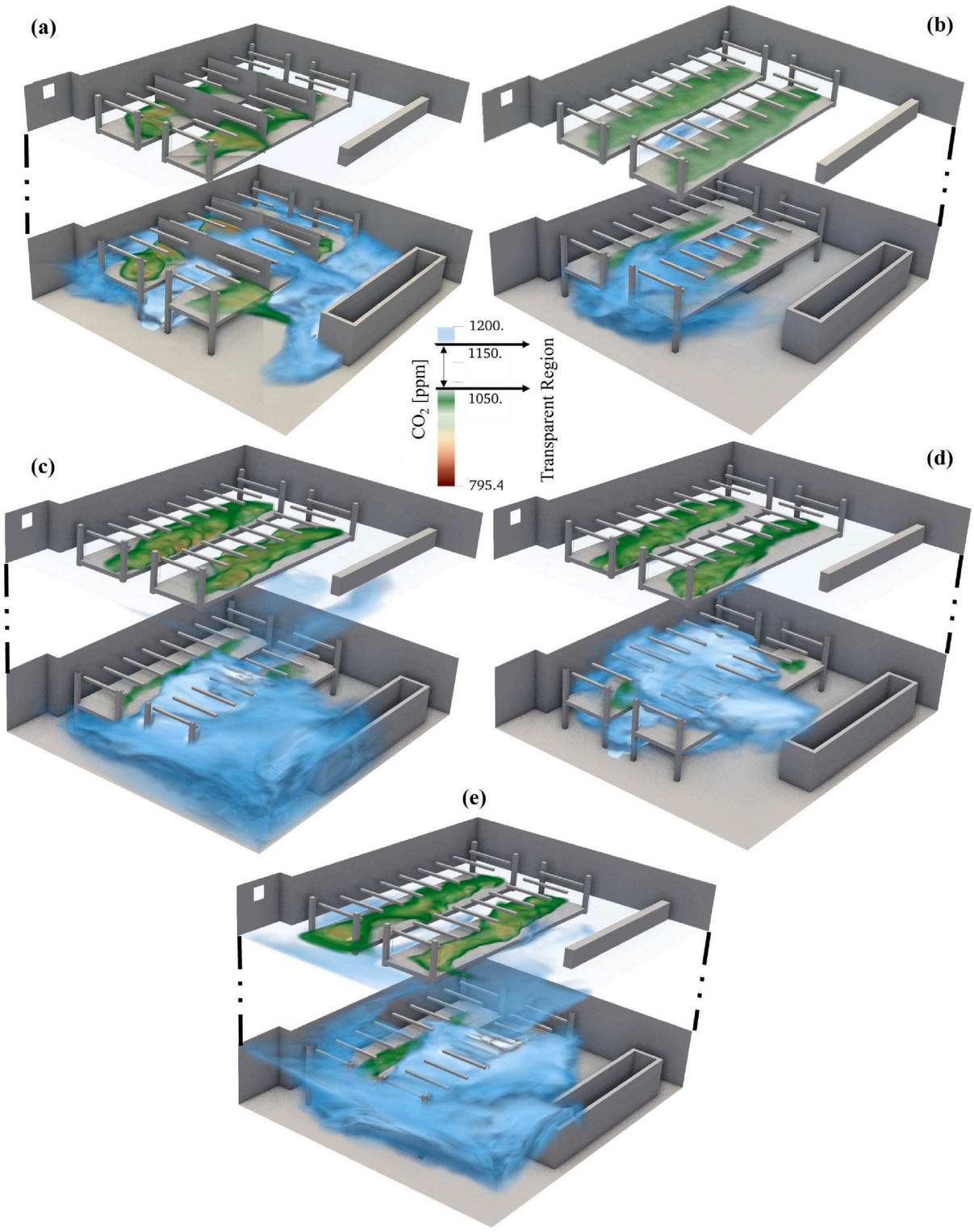

Fig. 3. 3D volume rendering of CO_2 propagation for: (a) case I, (b) case II, (c) case III, (d) case IV, and (e) case V. For a better visualisation, the second floor is artificially lifted up from the first floor.

result, the horizontal near-wall circulation existing on the first floor is weaker on the second floor, and the positive buoyant flow between the two shelves (cf. Fig. 6, subset v) transfers the flow towards the ceiling of the system. Moreover, in the absence of a strong horizontal circulation on the second floor, the entrainment in the vicinity of the dehumidifier causes the airflow to travel towards the dehumidifier region (vi). In conclusion, the dehumidifier region has a crucial impact on the airflow within the system as a result of its role in both vertical and horizontal airflow circulation within the system.

3.3.3. *Airflow effect on the mass transport*

Here, we discuss the CO_2 concentration field within the IVFAL and how the flow field is affecting it. Fig. 6 shows the time-averaged velocity streamlines along with CO_2 concentration, 15 cm above the

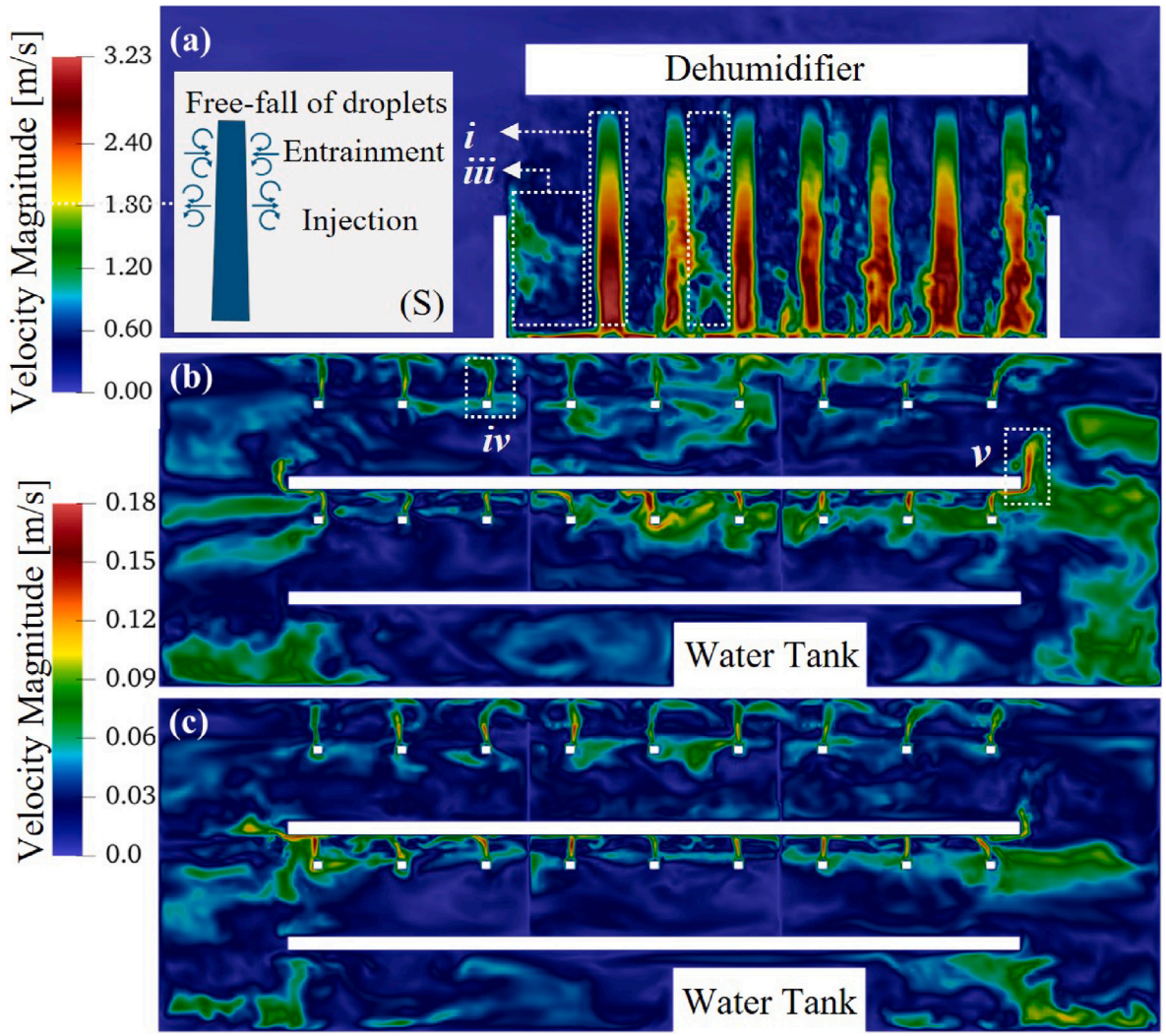

Fig. 4. Instantaneous velocity field in cross sections (a) zy3, (b) zy2, and (c) zy1 in case I, along with (S) schematic of the momentum injection mechanism. i: primary airflow induced by free-falling droplets. ii: shear-stress driven lateral secondary flow, specifically in the jet boundary. iii: wall-confinement induced axial secondary flow. iv: positive buoyancy around LED lamps. v: trapped positive buoyant flow beneath the second floor. For the definition of slices, cf. Fig. 2. (For interpretation of the references to colour in this figure legend, the reader is referred to the web version of this article.)

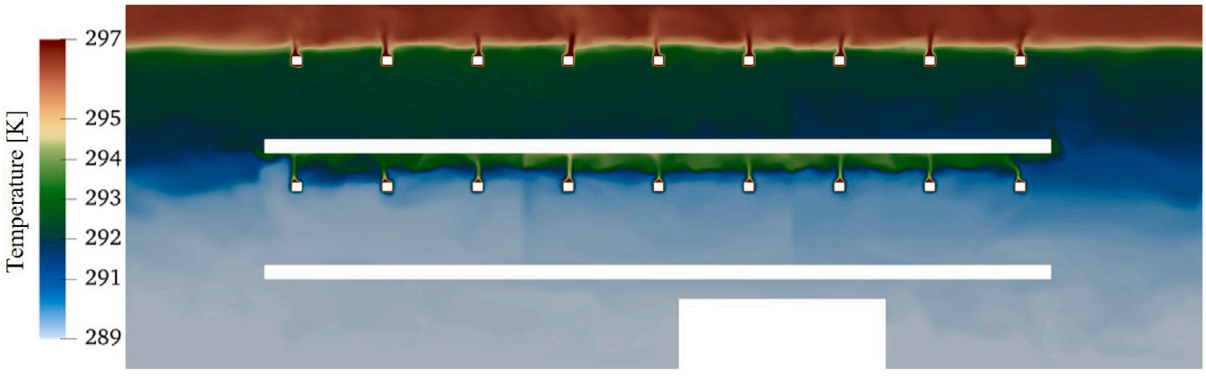

Fig. 5. Stratification of temperature in the vertical farm based on case I, plane zy2. For the definition of slices, cf. Fig. 2.

cultivation beds. In addition to the described horizontal circulations near the walls, there are local circulations above the cultivation beds on both floors. The local circulation in Region 3, Fig. 6(c) (i), and Region 9 (d) (i), are anticlockwise inward circulations, which transfer the flow towards the cultivation beds in these regions, leading to higher consumption of CO_2 in these zones. On the contrary, the outward circulation in Region 2 facilitates the vertical transportation of the flow and precludes the over-consumption of CO_2. Additionally, the confinement effect of the curtains in Region 5 (Fig. 6(c) subset iii) results in parallel streamlines above the cultivation beds, resulting in better mass transport in this region. Another effect of the curtains is where the streamlines are perpendicular to the curtains, resulting in

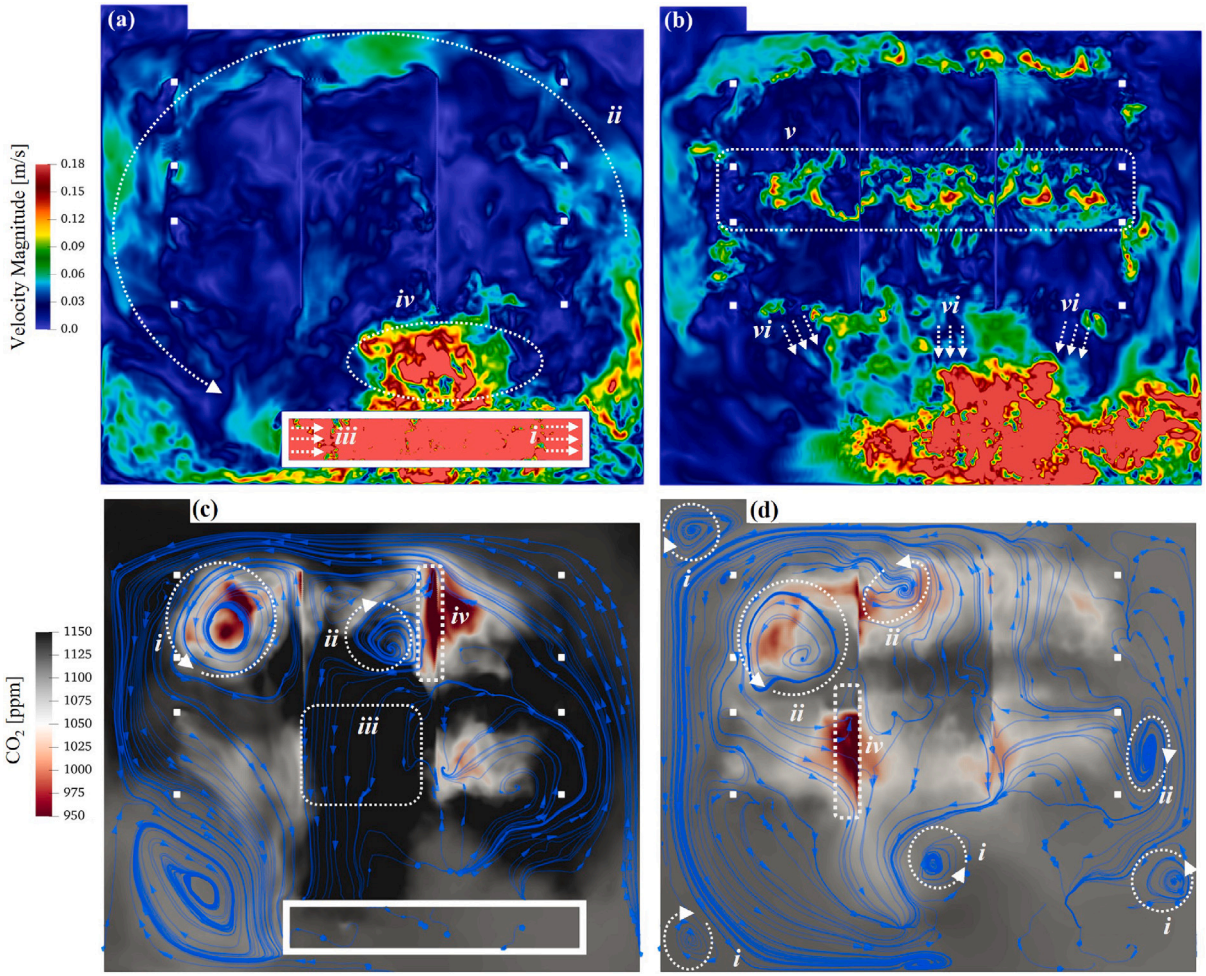

Fig. 6. Velocity field on (a) the first floor plane, xy1, and (b) the second floor plane, xy2. i: droplet free-fall induced momentum injection, ii: momentum injection driven anticlockwise horizontal circulation, iii: entrainment of the airflow to the dehumidifier region, iv: negative and positive buoyancy interaction, v: positive buoyant flow between two cultivation beds, vi: entrainment of the airflow towards the dehumidifier region. For the definition of slices, cf. Fig. 2.

stagnation regions close to the curtains and reduction of mass exchange, specifically, at zone (iv) on the first floor and zone (ii) on the second floor. Moreover, comparing the circulation zones near and far from the dehumidifier on the second floor shows that all the circulations near the dehumidifier are inward, resulting in the transfer of airflow to the lower height levels, while most of the circulation zones far from the dehumidifier are outward, illustrating the effect of positive buoyancy. This observation further supports the role of droplets' free fall in the vertical circulation within the vertical farm.

3.4. Effect of curtains on the airflow and mass transport

Fig. 7 shows the average distribution of CO_2 as bars and RH as dashed lines for each region (regions are indicated in Fig. 2) for cases with curtains (case I, coloured as blue) and without curtain (case II, coloured as red). The x-axis shows the regions with numbers while the vertical left and right axes show normalised CO_2, and RH, respectively. CO_2 is normalised with the released concentration of CO_2 at the distributor pipe, while RH is normalised based on the total amount of humidity release from the cultivation beds. Generally, in eight out of twelve regions, CO_2 is up to 8% lower in the case with curtains. Similarly, in ten regions RH is up to 7% higher in the case with curtain, suggesting lower mass transport in the presence of the curtains within the vertical farm. Exceptionally, in region five, the lower concentration of RH, and higher concentration of CO_2 indicate better mass transport in the case with curtains for this region. The airflow parallel to the curtains facilitates the mass transport. Region five is longitudinally confined with two curtains, a dehumidifier on one lateral side and the carbon dioxide distributor pipe on the other side. Two curtains prevent the longitudinal propagation of the CO_2, leading to the parallel alignment of airflow and the curtains, resulting in the highest CO_2 accumulation in this region.

3.5. Impact of light arrangements on the airflow and mass transport

In this section, we analyse the effect of light arrangements on the airflow. Each block contains 12 lamps (see Fig. 2 for the definition of blocks). According to Table 1, all across the blocks are operative in cases I and II, whereas in cases III, IV, and V, lamps above two blocks are operative. In what follows, first, we provide qualitative results of the velocity and CO_2 fields above the cultivation beds for cases II and IV to assess the impact of light intensity. Then, a quantitative comparison of CO_2 and RH in each region for all the cases with different light arrangements is represented and discussed. These qualitative and quantitative analyses focus on the mass transport and airflow within the regions of interest, i.e. the cultivation beds. Finally, to conclude on the effect of environmental factors (both effects of curtains and LED lamps arrangement) on the entire IVFAL systems, the density pair plot of CO_2 and RH is represented and discussed for all cases.

In case II, compared to case IV, more LED lamps operate, and consequently, more heat is released within the system. Therefore, the positive buoyancy is stronger in case II, which facilitates the vertical

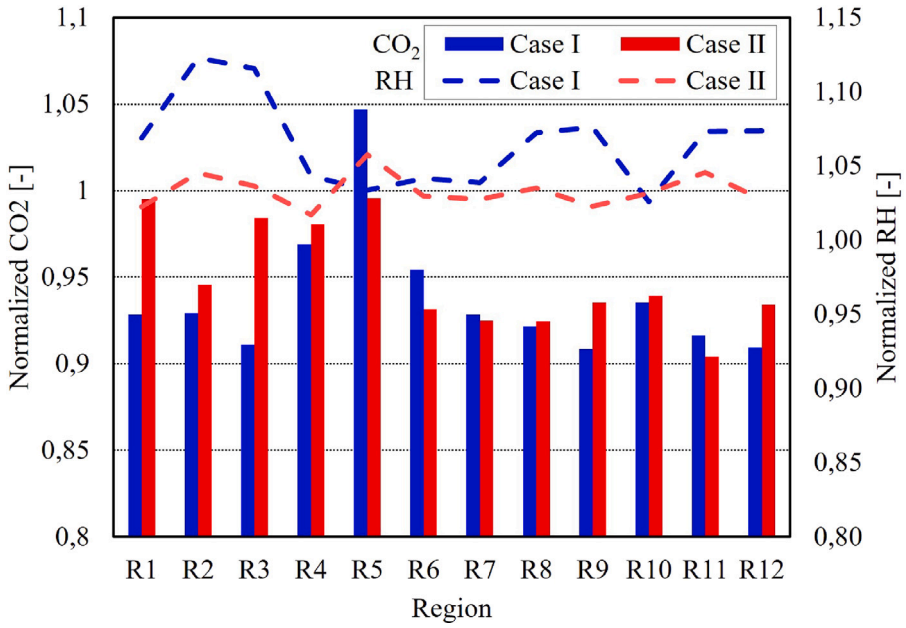

Fig. 7. CO_2 for cases I and II curtains based on regions 1 to 6 on the first floor, and regions 7 to 12 on the second floor. The bars correspond to the CO_2 and the dashed lines represent the trend of increase and decrease of RH between regions. Values of each region in abscissa are provided in normalised averaged CO_2 on the left ordinate and normalised averaged RH on the right ordinate axis. For the definition of regions, cf. Fig. 2. (For interpretation of the references to colour in this figure legend, the reader is referred to the web version of this article.)

transport of momentum, leading to a more homogeneous velocity field in this case. The stronger interaction between negative and positive buoyancy near the dehumidifier in the first floor of Case II, Fig. 8(a), subset i, than case IV, Fig. 8(c), subset i, suggests enhanced vertical transport in this region due to the more positive buoyant flow sources in Case II. The heated airflow by the lamps on the first trays is trapped below the structure of the second cultivation bed and then transfers to the upper part as bulks of the flow represented as spots in Fig. 8(c) and (d). The inclination of these spots indicates the direction of the airflow on the second floor (iii and iv). The inclination of the airflow towards the dehumidifier zone (iii) illustrates the entrainment of the flow on the second floor. Similarly to case I (with curtains), in case IV, horizontal circulation emerges close to the walls of the system, being stronger on the first floor (ii) and weaker on the second floor (iv).

Fig. 9 shows CO_2 accumulation over the cross-section planes of the first and second cultivation beds for case II (panels (a) and (b)) and case IV (panels (c) and (d)) on the first and second floor, respectively. In the colour scale, black represents the highest concentration, white covers the medium range, and red represents low concentration. The impact of velocity on the mass transport is highlighted by comparing the velocity field, cf. Fig. 8, to the CO_2 field, c.f. Fig. 9. Similar to the velocity magnitude field, the CO_2 field shows a higher concentration on the first floor of case IV compared to case II (Fig. 9(a) vs. (c)), and lower concentration on the second floor (Fig. 9(b) vs. (d)). This difference arises due to the imbalance of positive and negative buoyancy in the system. In case IV, the lamps in the middle of the system (regions 2 and 4) are not operational, resulting in no heat flux to induce vertical mass transport in those regions. However, the negative buoyancy and shear stress of droplets transfer the airflow from the second floor down to the first floor. Subsequently, the portion of CO_2 that remains unconsumed by plants on the second floor accumulates with the CO_2 released by the supplier on the first floor, leading to a higher concentration in the first floor of Case IV.

Fig. 10 provides quantitative results of the CO_2 accumulation and RH levels. In all regions of the first floor (regions one to six), the amount of CO_2 is higher than that of the second floor. Conversely, RH is generally lower on the first floor than on the second floor. Moreover, for cases III, IV and V, the cultivation beds on the second floor have 8%, 5% and 7% higher RH, respectively, compared to the first cultivation beds. Due to the lower positive buoyancy, Case III exhibits less mass transport than Cases IV and V. In Case III, the location of positive buoyancy sources to Region 4, where the momentum injection occurs on the first floor, is the farthest, resulting in less mass transport to the second floor in this case. Moreover, the impediment of the second cultivation bed structure to the positive buoyancy of the lamps on the first floor reduces the upward mass transport. This impediment is more effective in Block 2, where the trapped positive buoyancy has two edges to escape upward, while in the other two Blocks, the positive buoyant flow experiences less impediment as it can travel upward from three edges of the second cultivation bed. Therefore, the impediment affects Case IV less than Cases III, and V, resulting in more mass transport to the second floor. To conclude, Case IV has the best mass transport performance among cases with 24 operative lamps due to the less confinement of positive buoyant flow by the second cultivation bed, and overlap of the positive buoyant and momentum injection zone in the first floor.

Analysing the propagation of carbon dioxide and relative humidity in the whole system provides a comprehensive insight into the influence of environmental factors on mass transport. Fig. 11 presents a RH-CO_2 pair plot for the entire domain. The value of RH and CO_2 for each of the 14.1×10^6 computational cells in the domain are represented as a point in the graph, resulting in the demonstrated cloud data. The extracted values are clustered based on their location in the system. This clustering is depicted in the legend and the computational domain, which is represented in Fig. 11. The base, first and second floors, along with the dehumidifier zone, are coloured green, red, grey and blue. Additionally, the data clouds are shown transparently to visualise the overlaps of the points in graphs.

In the first and second floors of all cases, a negative correlation exists between RH and CO_2 due to plants' transpiration/photosynthesis. However, CO_2 varies in a nearly constant humidity in the base floor zone. CO_2 peaks at the highest concentration in this zone as the upward mass transport is relatively weak, and the CO_2 supplier is located on this floor, while there is no production/consumption of humidity in this floor, resulting in a constant value for RH. Besides the trends, the humidity and carbon dioxide distribution range can be interpreted as the uniformity of mass propagation. The wider the distribution range,

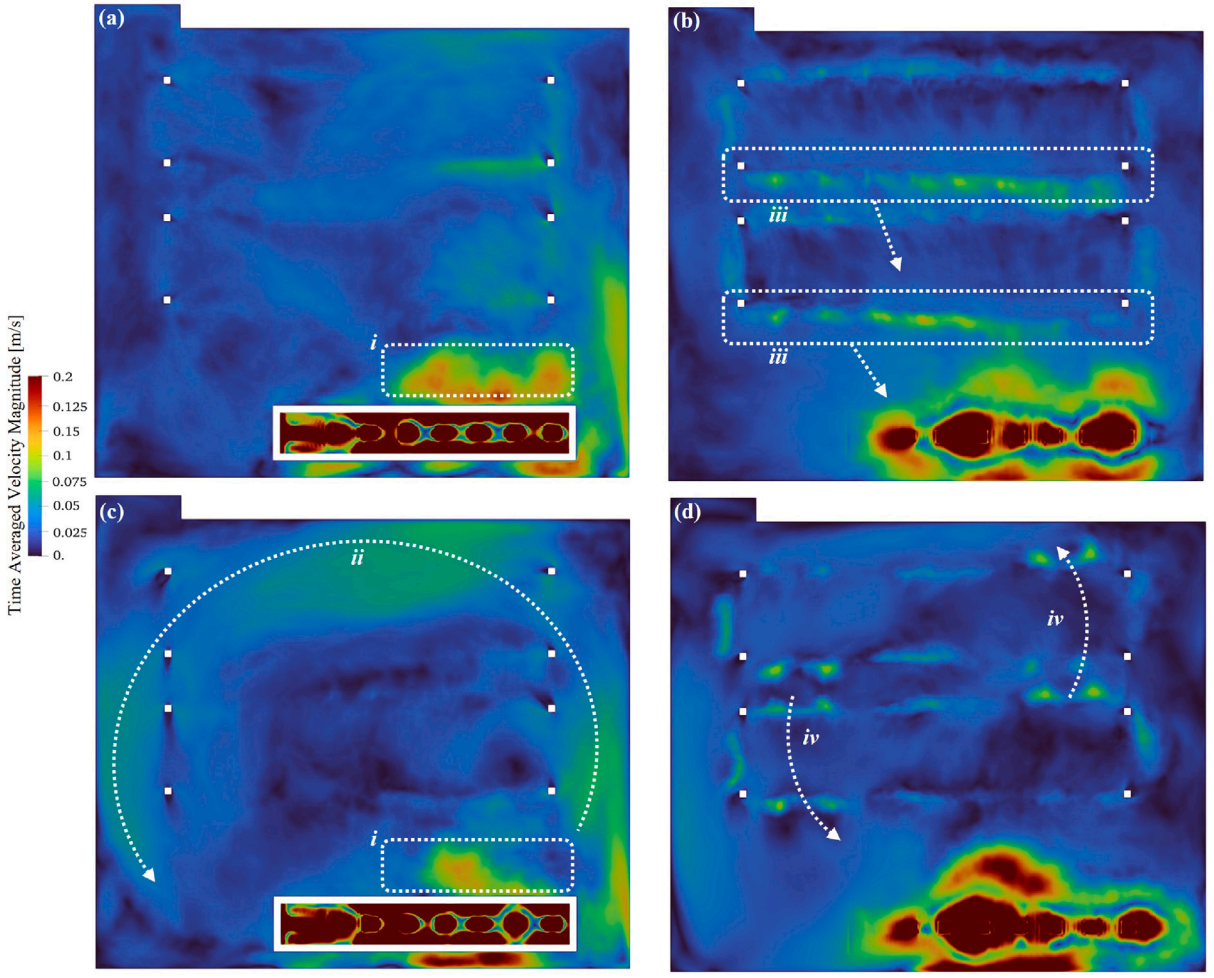

Fig. 8. Time averaged velocity magnitude for case II in the (a) first and (b) second floor, along with case IV in the (c) first and (d) second floor. i: the positive and negative buoyancy interaction, ii: the first floor horizontal circulation, iii: buoyancy-induced flows inclining towards the dehumidifier region, iv: the second floor horizontal circulation.

the lower the uniformity. In this regard, the best mass propagation uniformity belongs to Case II. While the mass distribution in Case II shows similar patterns in the first and second floors, in Case I, a higher distribution (lower uniformity) occurs on the first floor, and in Cases III to V, a higher distribution (lower uniformity) occurs on the second floor. Comparing the distribution difference between Case I and other cases highlights the impact of environmental factors on mass transport. The curtains have a more severe effect on mass transport than reducing the number of operative lamps.

3.6. Considerations of guide practitioners and suggestions for future studies

Although the present study focuses on evaluating fluid flow characteristics rather than developing a full design, several insights can be followed in future studies, and under consideration of a guide for practitioners in optimising vertical farm systems.

3.6.1. Tray configuration

Enclosing the cultivation beds on three sides by using two vertical plates and a horizontal plate above (the underside of the upper cultivation bed can serve this role) leads to parallel streamlines of airflow, enhancing the mass exchange above cultivation beds. The front and back remain open to act as air inlets and outlets. This arrangement increases mass exchange above the cultivation beds.

3.6.2. Airflow pathways

Locating solid structures where they would obstruct major airflow streams should be avoided. Interruptions in the airflow reduce mass exchange and limit the uniform distribution of fresh air around the crops.

3.6.3. Lamp placement

Lamps can enhance vertical mass transport by increasing the temperature and enhancing upward buoyancy-driven flows. Although, if horizontal structures trap heat above the lamps, this effect would be mitigated. Moreover, locating lamps near airflow inlets to the system increases vertical momentum transfer to the upper floors.

These practical considerations provide a starting point for implementation but require further investigation under diverse design and operational conditions.

4. Conclusion

In this study, we investigate the buoyancy-driven airflow behaviour within a laboratory-scale vertical farm, using the LES turbulence modelling approach, SGS turbulence model of Yoshizawa, and simulating the free-fall of droplets with the Eulerian-Lagrangian approach. To the best of the author's knowledge, this is the first LES setup simulating vertical farm ventilation. The enthalpy equation has been solved to provide the buoyancy effect on the airflow, and passive scalar transport equations were governed by the mass transport of RH and CO_2.

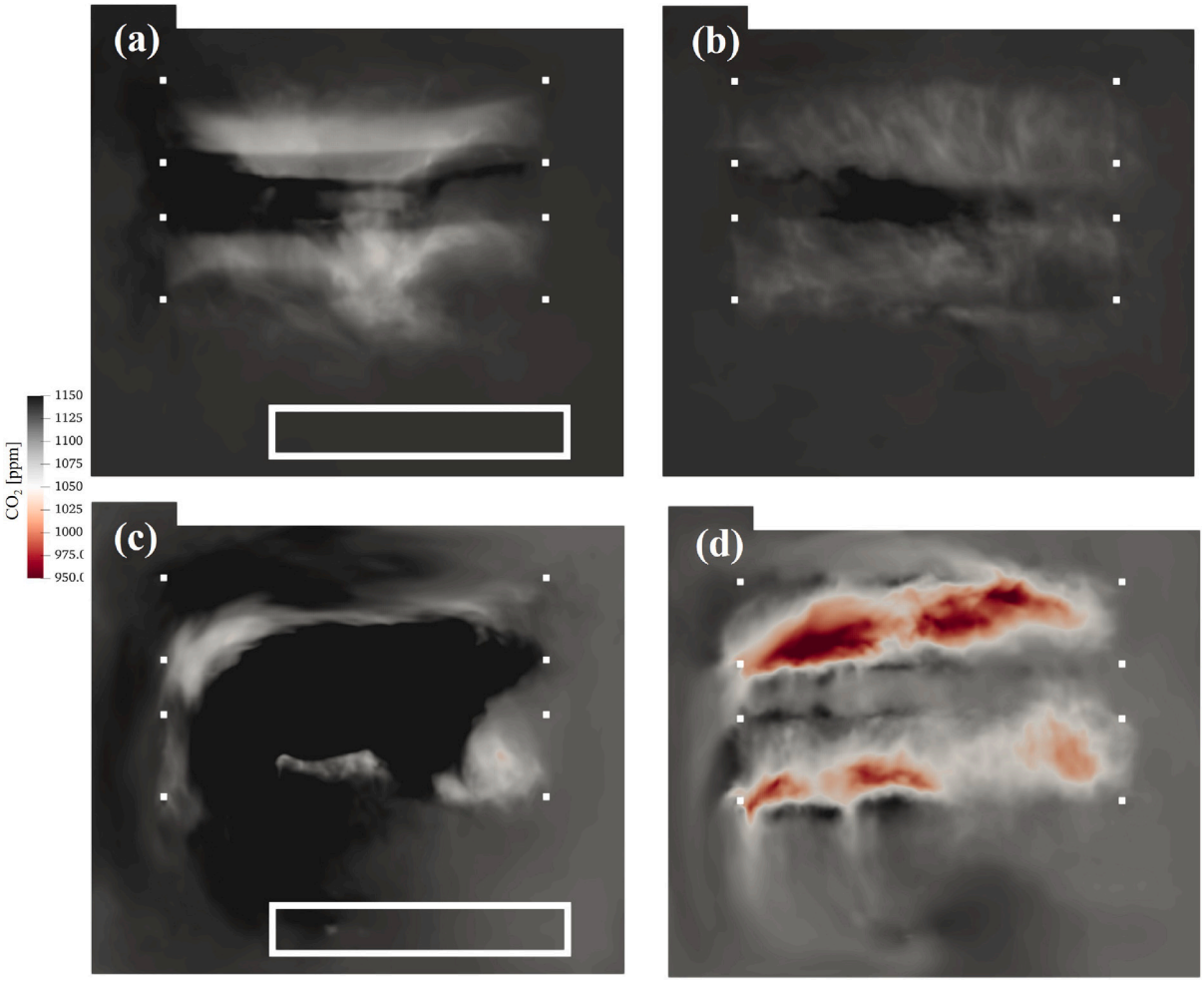

Fig. 9. CO_2 concentration in case II above (a) the first and (b) the second floor, as well as in case IV above (c) the first, and (d) the second floor. (For interpretation of the references to colour in this figure legend, the reader is referred to the web version of this article.)

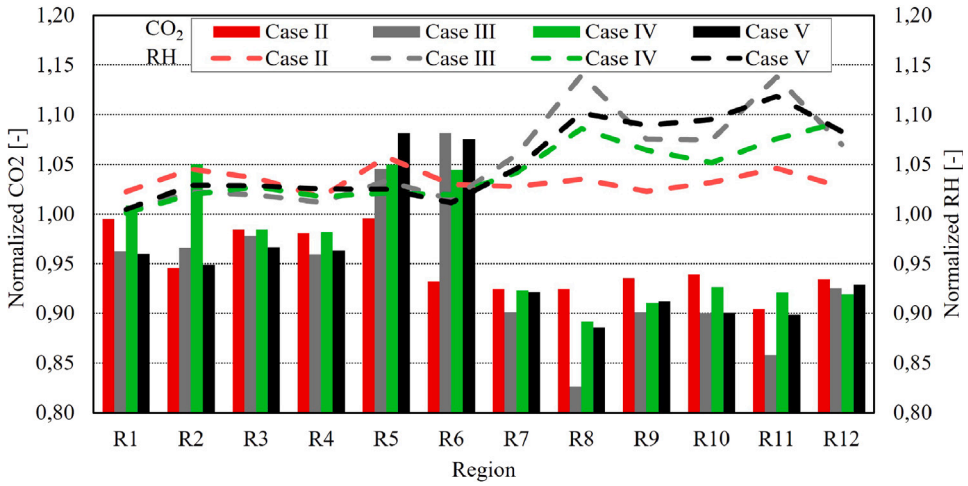

Fig. 10. Average normalised CO_2 and RH among regions in each case with various light configurations. Normalisation has been done based on the injected CO_2, and total release of RH by cultivation beds for CO_2 and RH subsequently. The bars correspond to the CO_2 and the lines represent the trend of increase and decrease of RH between regions. Values of each region in abscissa are provided in normalised averaged CO_2 on the left ordinate and RH on the right ordinate axis. For the definition of regions, cf. Fig. 2.

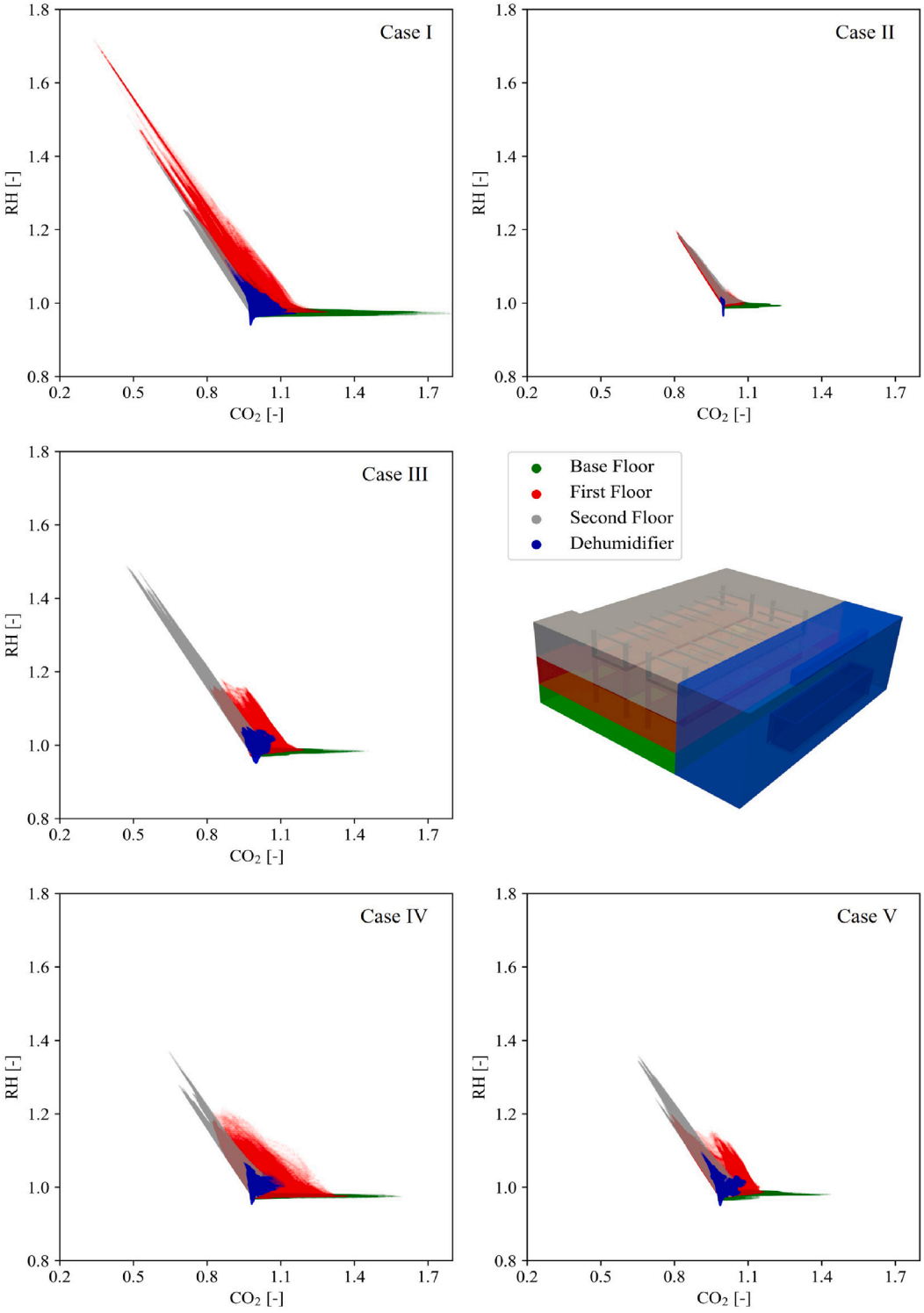

Fig. 11. Pair plot of RH-CO_2 based on point clouds of all computational cells in the vertical farm for all cases. Data has been clustered based on the various locations in the vertical farm, specified in the legend and computational domain. (For interpretation of the references to colour in this figure legend, the reader is referred to the web version of this article.)

The aim was to highlight the effect of environmental factors, such as wall-confinement, positive buoyancy of LED lamps, and negative buoyancy of a cooling system, on the airflow as well as mass transport in an indoor agricultural system with artificial lighting. In the absence of mechanical ventilation, the airflow is mainly affected by positive buoyancy, driven by the heat release from the lamps, and by the negative buoyancy, driven by the cooling system, as well as the shear stress exchange of droplets with the airflow. The LES simulations were conducted prior to our experimental campaign, providing a blind method validation of the numerical setup with experimental conditions. Temperature, humidity, and CO_2 were predicted with the mean absolute error of 0.82%, 2.22%, and 3.96%, respectively, showing a good agreement between the LES numerical setup and the experimental measurement. The analysis of the instantaneous airflow

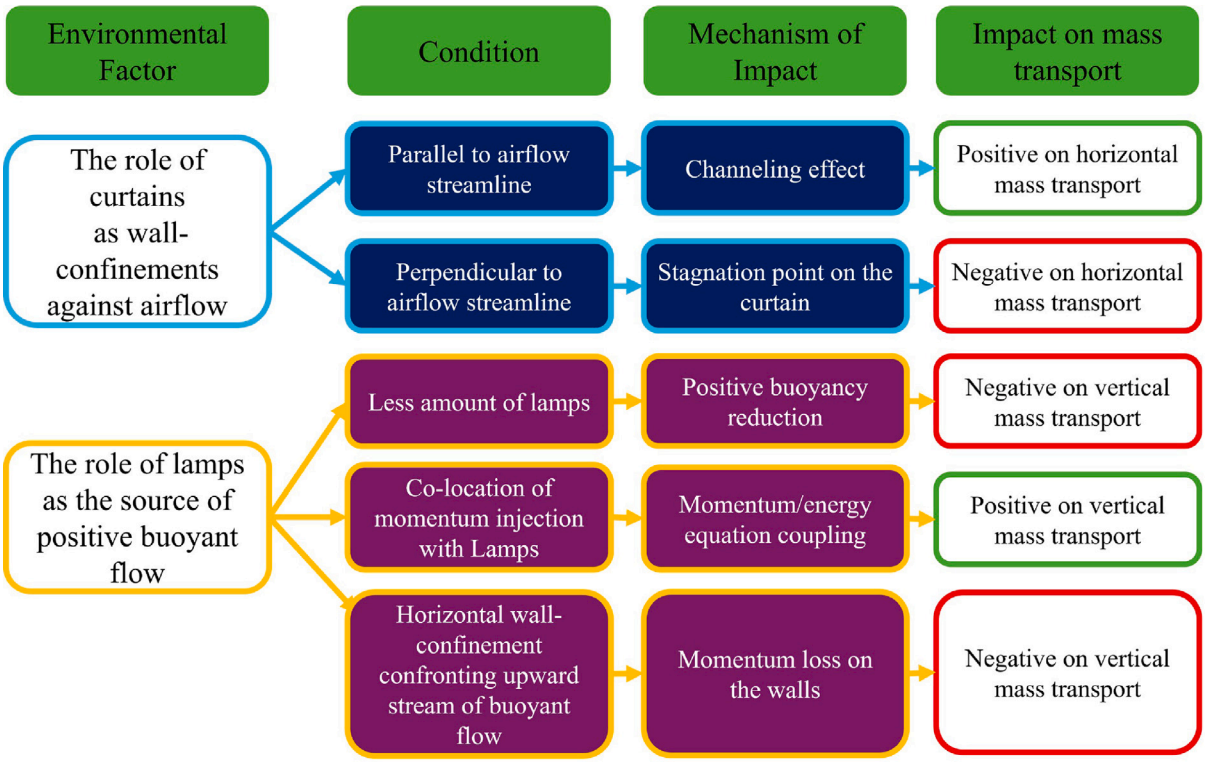

Fig. 12. A summary of the environmental factors' impact on the mass transport within the vertical farm.

above the cultivation beds showed a critical impact from the free-falling droplets on the vertical and horizontal airflow within the whole vertical farm. A summary of the findings based on environmental factors represented in Fig. 12. Curtains generally had an adverse effect on the mass transport above the cultivation beds. As such, the wall confinement of the curtains was not beneficial for the growth of plants. However, their effect on mass transport depends on the angle between the curtain and the airflow. A perpendicular airflow to the curtain reduces the mass transport in the majority of the regions, while a parallel airflow to the curtain enhances the mass transport due to the channelling effect. Reducing the number of operative lamps resulted in inhomogeneous vertical mass propagation due to the weak positive buoyancy effect. The heat release of lamps results in a positive buoyant flow, facilitating upward vertical mass transport. Two factors were associated with the enhancement of the positive buoyant flow based on shifting the location of the lamps. The proximity of the lamps to the momentum injection zone had a positive effect on vertical mass transport, while the confrontation of the positive buoyant flow with the wall beneath the second cultivation bed had a negative effect on the vertical mass transport. From best to worst, uniformity of CO_2 propagation has been observed for cases II, IV, III, V, and I.

CRediT authorship contribution statement

Ali A. Ashnani: Writing – review & editing, Writing – original draft, Visualization, Validation, Software, Methodology, Formal analysis. **Alpo Laitinen:** Writing – review & editing, Visualization, Software, Methodology, Investigation, Conceptualization. **Shervin Karimkashi:** Writing – review & editing. **Ville Vuorinen:** Writing – review & editing. **Titta Kotilainen:** Writing – review & editing, Resources. **Juha Näkkilä:** Resources, Investigation. **Pasi Herranen:** Writing – review & editing, Resources. **Ossi Kaario:** Writing – review & editing, Supervision, Project administration, Funding acquisition, Conceptualization.

Declaration of competing interest

The authors declare that they have no known competing financial interests or personal relationships that could have appeared to influence the work reported in this paper.

Acknowledgements

We thank the cooperation of technicians at the LUKE Piikkiö research station for their practical assistance during the study. Special thanks to Olli Ranta for assisting us with the experimental campaign. The computational resources of the study were provided by CSC Finnish IT Center for Science.

Appendix A. Supplementary data

Supplementary material related to this article can be found online at https://doi.org/10.1016/j.ijheatmasstransfer.2025.127964.

Data availability

All data and Information is available based on requesting, excluding the geometry source file of the study.

References

[1] T. Kozai, Resource use efficiency of closed plant production system with artificial light: Concept, estimation and application to plant factory, Proc. Jpn. Acad. Ser. B: Phys. Biological Sci. 89 (2013) http://dx.doi.org/10.2183/pjab.89.447.
[2] D.D. Avgoustaki, G. Xydis, Plant factories in the water-food-energy nexus era: a systematic bibliographical review, Food Secur. 12 (2020) http://dx.doi.org/10.1007/s12571-019-01003-z.
[3] C. Vatistas, D.D. Avgoustaki, T. Bartzanas, A systematic literature review on controlled-environment agriculture: How vertical farms and greenhouses can influence the sustainability and footprint of urban microclimate with local food production, Atmosphere 13 (2022) http://dx.doi.org/10.3390/atmos13081258.

[4] P. Thongbai, T. Kozai, K. Ohyama, Co_2 and air circulation effects on photosynthesis and transpiration of tomato seedlings, Sci. Hort. 126 (2010) http://dx.doi.org/10.1016/j.scienta.2010.07.018.
[5] T. Shibuya, J. Tsuruyama, Y. Kitaya, M. Kiyota, Enhancement of photosynthesis and growth of tomato seedlings by forced ventilation within the canopy, Sci. Hort. 109 (2006) http://dx.doi.org/10.1016/J.SCIENTA.2006.04.009.
[6] Q. Mao, H. Li, C. Ji, Y. Peng, T. Li, Experimental study of ambient temperature and humidity distribution in large multi-span greenhouse based on different crop heights and ventilation conditions, Appl. Therm. Eng. 248 (2024) http://dx.doi.org/10.1016/j.applthermaleng.2024.123176.
[7] Q. Mao, C. Ji, H. Li, Y. Peng, T. Li, Dynamic temperature distribution characteristics of a large glasshouse with cooling system during the start-stop stage, Comput. Electron. Agric. 220 (2024) http://dx.doi.org/10.1016/j.compag.2024.108913.
[8] Y. Kitaya, Importance of air movement for promoting gas and heat exchanges between plants and atmosphere under controlled environments, in: Plant Responses to Air Pollution and Global Change, Springer, Japan, Tokyo, 2005, pp. 185–193, http://dx.doi.org/10.1007/4-431-31014-2_21.
[9] H.A. Ahmed, Y.-X. Tong, Q.-C. Yang, Optimal control of environmental conditions affecting lettuce plant growth in a controlled environment with artificial lighting: A review, S. Afr. J. Bot. 130 (2020) http://dx.doi.org/10.1016/J.SAJB.2019.12.018.
[10] P.E. Bournet, F. Rojano, Advances of computational fluid dynamics (CFD) applications in agricultural building modelling: Research, applications and challenges, Comput. Electron. Agric. 201 (2022) http://dx.doi.org/10.1016/J.COMPAG.2022.107277.
[11] H. Fatnassi, T. Boulard, J.C. Roy, R. Suay, C. Poncet, CFD coupled modeling of distributed plant activity and climate in greenhouse, Acta Hortic. 1182 (2017) http://dx.doi.org/10.17660/ActaHortic.2017.1182.6.
[12] A.G. Niam, T.R. Muharam, S. Widodo, M. Solahudin, L. Sucahyo, CFD simulation approach in determining air conditioners position in the mini plant factory for shallot seed production, AIP Conf. Proc. 2062 (2019) http://dx.doi.org/10.1063/1.5086564.
[13] A. Mohd Noh, M.A. Mohamad Tahir, S. Mat, M.H. Dzulkifli, CFD simulation of temperature and airflow inside a shipping container size plant factory for optimal lettuce production, Food Res. 4 (2020) http://dx.doi.org/10.26656/fr.2017.4(S6).039.
[14] T.-G. Lim, Y.H. Kim, Analysis of airflow pattern in plant factory with different inlet and outlet locations using computational fluid dynamics, J. Biosyst. Eng. 39 (2014) http://dx.doi.org/10.5307/jbe.2014.39.4.310.
[15] Y. Zhang, M. Kacira, L. An, A CFD study on improving air flow uniformity in indoor plant factory system, Biosyst. Eng. 147 (2016) http://dx.doi.org/10.1016/j.biosystemseng.2016.04.012.
[16] H. Fang, K. Li, G. Wu, R. Cheng, Y. Zhang, Q. Yang, A CFD analysis on improving lettuce canopy airflow distribution in a plant factory considering the crop resistance and LEDs heat dissipation, Biosyst. Eng. 200 (2020) http://dx.doi.org/10.1016/j.biosystemseng.2020.08.017.
[17] Y. Zhang, M. Kacira, Analysis of climate uniformity in indoor plant factory system with computational fluid dynamics (CFD), Biosyst. Eng. 220 (2022) http://dx.doi.org/10.1016/j.biosystemseng.2022.05.009.
[18] B. Naranjani, Z. Najafianashrafi, C. Pascual, I. Agulto, P.Y.A. Chuang, Computational analysis of the environment in an indoor vertical farming system, Int. J. Heat Mass Transfer 186 (2022) http://dx.doi.org/10.1016/j.ijheatmasstransfer.2021.122460.
[19] J. Sohn, M. Liulys, D.D. Avgoustaki, G. Xydis, CFD analysis of airflow uniformity in a shipping-container vertical farm, Comput. Electron. Agric. 215 (2023) http://dx.doi.org/10.1016/J.COMPAG.2023.108363.
[20] G. Larochelle Martin, D. Monfet, High-density controlled environment agriculture (CEA-HD) air distribution optimization using computational fluid dynamics (CFD), Eng. Appl. Comput. Fluid Mech. 18 (2024) http://dx.doi.org/10.1080/19942060.2023.2297027.
[21] G. Agati, B. Franchetti, F. Rispoli, P. Venturini, Thermo-fluid dynamic analysis of the air flow inside an indoor vertical farming system, Appl. Therm. Eng. 236 (2024) http://dx.doi.org/10.1016/j.applthermaleng.2023.121553.
[22] P.E. Bournet, T. Boulard, Effect of ventilator configuration on the distributed climate of greenhouses: A review of experimental and CFD studies, Comput. Electron. Agric. 74 (2010) http://dx.doi.org/10.1016/J.COMPAG.2010.08.007.
[23] B. Blocken, LES over RANS in building simulation for outdoor and indoor applications: A foregone conclusion? Build. Simul. 11 (2018) http://dx.doi.org/10.1007/s12273-018-0459-3.
[24] M. Su, Q. Chen, C.M. Chiang, Comparison of different subgrid-scale models of large eddy simulation for indoor airflow modeling, J. Fluids Eng. 123 (2001) http://dx.doi.org/10.1115/1.1378294.
[25] M. Korhonen, A. Laitinen, G.E. Isitman, J.L. Jimenez, V. Vuorinen, A GPU-accelerated computational fluid dynamics solver for assessing shear-driven indoor airflow and virus transmission by scale-resolved simulations, J. Comput. Sci. 78 (2024) http://dx.doi.org/10.1016/J.JOCS.2024.102265.
[26] A. Yoshizawa, Statistical theory for compressible turbulent shear flows, with the application to subgrid modeling, Phys. Fluids 29 (1986) http://dx.doi.org/10.1063/1.865552.
[27] A. Laitinen, M. Korhonen, K. Keskinen, O. Kaario, V. Vuorinen, Large-eddy simulation of buoyant airflow in an airborne pathogen transmission scenario, Build. Environ. 241 (2023) http://dx.doi.org/10.1016/j.buildenv.2023.110462.
[28] D. Piscia, J.I. Montero, B. Bailey, P. Muñoz, A. Oliva, A new optimisation methodology used to study the effect of cover properties on night-time greenhouse climate, Biosyst. Eng. 116 (2013) http://dx.doi.org/10.1016/J.BIOSYSTEMSENG.2013.07.005.